Desalination 582 (2024) 117624

Contents lists available at ScienceDirect

Desalination

journal homepage: www.elsevier.com/locate/desal

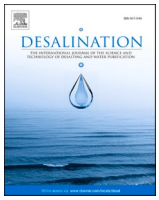

Techno-economic feasibility of photovoltaic solar electrodialysis with bipolar membranes

Marta Herrero-Gonzalez [a,b,*], Andrea Culcasi [b], Alessandro Tamburini [b], Raquel Ibañez [a], Andrea Cipollina [b,**], Giorgio Micale [b]

[a] Departamento de Ingenierías Química y Biomolecular, Universidad de Cantabria, Avda. Los Castros s/n, 39005 Santander, Cantabria, Spain
[b] Dipartimento di Ingegneria, Università degli Studi di Palermo, Viale delle Scienze ed. 6, 90128 Palermo, Italy

HIGHLIGHTS

- A novel integrated PV-EDBM model was developed and applied to brine valorization.
- NaOH productivity, SEC and CE of grid mix and PV solar powered EDBM compared
- Replacing the grid mix by PV solar resulted in similar productivity, SEC and CE.
- Using PV solar energy reduces LCoNaOH by about 20 % during the solar year.
- PV-EDBM reduces GHG emissions, avoiding costs of carbon tax and EU ETS allowances.

ARTICLE INFO

Keywords:
Renewable energy
Process integration
Poly generation systems
Electro-membrane
Ion exchange membranes

ABSTRACT

Electrodialysis with bipolar membranes (EDBM) can transform concentrated brines into acids and bases through the application of an electric field. Nevertheless, the widespread use of EDBM is limited by its high energy consumption, typically based on fossil fuels. Yet, the integration of EDBM with renewable energy sources, like solar photovoltaic (PV), remains unexplored. This study presents a techno-economic analysis of PV-EDBM to produce NaOH and HCl from seawater reverse osmosis (SWRO) brines. An integrated PV-EDBM model was developed and applied to a hypothetical PV-EDBM plant located in the SWRO facility of Lampedusa (Italy). Results revealed that PV has no negative impact on the performance in terms of product concentration, specific energy consumption and current efficiency. Meanwhile, the levelized cost of NaOH for PV-EDBM was reduced by 20 % in comparison to the electrical grid mix, achieving 210 €·ton^{-1} NaOH on an annual average for PV-EDBM. Therefore, the investment associated with PV is offset by the benefits of reduced electricity costs from the grid. Consequently, EDBM emerges as a feasible solution to address resource scarcity, representing a significant step towards integrating renewable energies with advanced wastewater treatment technologies, thus paving the path to a greener future.

Abbreviations: AEL, anion exchange layer; AEM, anionic exchange membrane; BPM, bipolar membrane; CE, current efficiency; CEL, cation exchange layer; CEM, cationic exchange membrane; ED, electrodialysis; EDBM, electrodialysis with bipolar membranes; EU ETS, European Union Emissions Trading System; GHG, greenhouse gas; LCoNaOH, levelized cost of NaOH; MLD, minimum liquid discharge; PV, photovoltaic; PV-ED, photovoltaic electrodialysis; PV-EDBM, photovoltaic electrodialysis with bipolar membranes; RO, reverse osmosis; SEC, specific energy consumption; SWRO, seawater reverse osmosis; TRL, technology readiness level; ZLD, zero liquid discharge.

* Correspondence to: M. Herrero-Gonzalez, Departamento de Ingenierías Química y Biomolecular, Universidad de Cantabria, Avda. Los Castros s/n, 39005 Santander, Cantabria, Spain.

** Correspondence to: A. Cipollina, Dipartimento di Ingegneria, Università degli Studi di Palermo, Viale delle Scienze ed. 6, 90128 Palermo, Italy.

E-mail addresses: herrerogma@unican.es (M. Herrero-Gonzalez), andrea.culcasi@unipa.it (A. Culcasi), alessandro.tamburini@unipa.it (A. Tamburini), raquel.ibanez@unican.es (R. Ibañez), andrea.cipollina@unipa.it (A. Cipollina), giorgiod.maria.micale@unipa.it (G. Micale).

https://doi.org/10.1016/j.desal.2024.117624
Received 27 November 2023; Received in revised form 8 April 2024; Accepted 9 April 2024
Available online 11 April 2024

1. Introduction

In a global context of resource and water scarcity [1–3], waste treatment and valorization chains emerged with the goal of recovering valuable products to ensure a sustainable supply. Attention is shifting towards transitioning from a linear economy concept to Circular Economy, where the consumption and waste of raw materials, water, and energy resources are minimized [4–9]. At the same time, the integration of renewable energy sources within industrial sectors such as water industry, is crucial for the decarbonization of such energy intensive processes. In this sense, most of the developed countries are implementing strategies to discourage CO_2 emissions into the atmosphere, such as carbon taxes and the EU Emissions Trading System (EU ETS) [10,11]. The first system aims to reduce high energy consumption, while the second aims to cap emissions.

Electro-membrane processes, such as electrodialysis (ED) or electrodialysis with bipolar membranes (EDBM), have gained popularity, either as the primary technology or as an auxiliary to other processes [12–15]. For instance, seawater reverse osmosis (SWRO) concentrates have demonstrated an enormous potential for material recovery, such as HCl and NaOH by means of EDBM, as well as energy recovery.

EDBM produces acids and bases from saline streams through an electric gradient. The main element for this technology is the stack, configured with anionic and cationic exchange membranes (AEM and CEM, respectively), together with bipolar membranes (BPM). AEM and CEM selectively transport anions and cations, respectively, across the membrane, while BPM promotes water dissociation under an electric field (following the second Wien effect) [16], generating protons (H^+) and hydroxide (OH^-) ions. Thus, saline streams could be valorized into acids and bases through EDBM. For instance, HCl and NaOH can be produced from synthetic NaCl solutions, but also from real waters or wastewaters such as SWRO brines (~1.0 mol·L^{-1} NaCl) [17,18]. From a Circular Economy perspective, these acids and bases could be employed within the facilities [19,20] or in other technologies involved in zero or minimum liquid discharge (ZLD/MLD) systems [21,22]. To provide an overview, it has been reported that, for a SWRO facility, the consumption rates are 0.2–0.5 g of HCl per cubic meter of freshwater, and 30–60 g of NaOH per cubic meter of freshwater [23].

While research and development of EDBM have focused on increasing the technology readiness level (TRL) [24–26] and modeling [27–30], its integration with renewable energies, despite being recommended, has seen limited exploration. This integration is crucial for reducing the environmental impacts associated with energy consumption, such as the indirect greenhouse gas (GHG) emissions, one of the main challenges of electro-membrane technologies [14,31]. EDBM energy consumption depends on membrane properties, especially their electrical resistance, due to the ohmic losses [32]. Energy consumption is also determined by the initial feed and product concentration. For instance, Yang et al. [33] produced 0.7 mol·L^{-1} HCl and 1.0 mol·L^{-1} NaOH from softened SWRO brines (0.65 mol·L^{-1} NaCl), with an energy consumption of 9.0 kWh·kg^{-1} HCl. In another study, 3.8 kWh·kg^{-1} HCl was required for the production of 1.99 mol·L^{-1} HCl and 2.14 mol·L^{-1} NaOH from pre-concentrated SWRO brines (3.42 mol·L^{-1} NaCl) [18]. 43.5 kWh·kg^{-1} HCl [23] (or 22.6 kWh·kg^{-1} NaOH [34]) was required to obtain 3.3 mol·L^{-1} HCl and 3.6 mol·L^{-1} NaOH. Although the reduction of specific energy consumption (SEC) remains an important challenge, the use of decarbonized energy sources is crucial to move forward to a more environmentally sustainable process.

The integration of ED technology with renewable energies, in particular photovoltaic solar (PV) and wind, has been extensively studied [35–37]. PV-ED has proven to be an outstanding alternative for sustainable desalination (freshwater production), especially when brackish water is used as feed stream, reporting lower energy consumptions than reverse osmosis (RO) [38]. PV-ED represents 9 % of the worldwide share of solar-powered desalination [39]. Savings of up to 0.724 kg CO_2-eq.·m^{-3} have been quantified for brackish water desalination through PV-ED compared to the electrical grid mix of Spain (emission factor of 0.223 kg CO_2-eq.·kWh^{-1}) [38]. The technical feasibility of PV-ED has been evaluated through experimental results [40,41] and mathematical models, which have been developed and validated [42–44].

On the other hand, the integration of renewable energies with EDBM is limited, mainly focusing on experimental results of PV-EDBM at a laboratory scale (TRL 4), achieving comparable performances to those powered by electrical grid mix [23,45]. Despite this fact, the potential for improving the environmental performance of PV-EDBM integration has been highlighted, with the ability to reduce indirect carbon emissions related to energy consumption to a tenth [23,34,46,47]. Nevertheless, an evaluation of the PV-EDBM integration is essential before scaling up.

In this regard, the present work aims to evaluate the feasibility of the integrated PV-EDBM process using a simulation platform. An integrated PV-EDBM model, based on existing literature models, has been developed and adopted for this purpose. Additionally, a techno-economic analysis was carried out to evaluate the current financial feasibility of a PV-EDBM installation.

2. Material and methods

2.1. Development of simulation tool: PV-EDBM integrated model

The integration of well validated PV and EDBM models was carried out using gPROMS Model Builder® platform [48].

The EDBM model is a comprehensive, semi-empirical tool with a multi-scale structure that accounts for all the major phenomena within the unit. This model, detailed and validated (with discrepancies below 3 %) in a previous work [27], encompasses four dimensional scales. The lowest scale is characterized by the channel and BPM models. The channel model predicts the chemical-physical properties of the electrolyte solutions using a database (OLI Studio®) and existing literature models. The BPM model forecasts the BPM function in terms of ion transport numbers and ion fluxes through the cation exchange layer (CEL) and anion exchange layer (AEL). The low-mid scale involves the repeating unit (triplet) and calculates the mass balances and fluxes through the monopolar membranes. Additionally, it computes primary electrical variables, such as the Nernst potential across the ion exchange membranes, the triplet's electrical resistance, and the boundary layer voltage drop due to concentration polarization. The medium-high scale focuses on the entire stack, comprising two sub-models: the parasitic currents sub-model and the hydraulics sub-model. The parasitic currents sub-model calculates the distribution of electric currents (including parasitic currents), in the representative equivalent electric circuit of the EDBM unit. The hydraulics sub-model focuses on fluid dynamics within the EDBM system and considers the flow distribution and pressure losses across the EDBM stack. The highest scale considers the external circuit, enabling predictions of dynamic mass balances in the external reservoirs of the electrolytic solutions and pressure losses across the external hydraulic circuit. This approach offers a more comprehensive understanding of the process, facilitating accurate predictions and the optimization of the unit's performance under various operating conditions.

On the other hand, the PV model was based on the "five parameters model" approach [49], known for its efficiency and accuracy, while keeping low computational time and load, in assessing PV systems performance [50]. Despite requiring five parameters which are not typically provided in the manufacturer's datasheet (i.e., photocurrent source, ideality factor and saturation current of the diode, and series (R_s) and shunt resistance (R_{sh}) of the PV cell), these can be calculated using other information provided by the manufacturer through different approaches [49–53]. Ibrahim and Anani [54] studied different analytical methods for the five parameters calculation, obtaining good results. Among them, a method where R_s and R_{sh} are neglected (i.e., $R_s = 0$ and

$R_{sh} = \infty$) has been selected in this work due to its simplicity, yet guaranteeing a good accuracy.

Energy balances have been included in the PV model [55] since the temperature of the module (in the junction) is not constant due to heat accumulation during operation. The energy balance of a PV panel considers the incoming shortwave solar radiation reaching the front surface of the PV panel, the electric power produced by the PV panel, and the heat transfer losses from the PV panel to the environment and vice versa. Losses from free and forced convection have been considered, while long-wave radiation has been neglected due to its lesser contribution and potential uncertainties in the calculation [55,56].

As depicted in Fig. 1, the integrated PV-EDBM model requires some input data and parameters related to the case of study, including EDBM stack and PV array size, operating time, initial solutions, and meteorology (location and period of the year). The connection between EDBM and PV models is stablished through Ohm's Law, which correlates the voltage and current provided by the PV array (calculated by the PV model) with the apparent electrical resistance of the EDBM unit (calculated by the EDBM model). The main outcomes derived from the integrated PV-EDBM are the concentration and volume of products (NaOH and HCl), specific energy consumption (SEC) and current efficiency (CE). Consequently, productivity and energy consumption can be quantified.

2.2. PV-EDBM simulation – Case of study description

An EDBM plant located on the island of Lampedusa (Italy), sharing similar characteristics with the one installed under the framework of EU-project WATER-MINING [57] and described in previous works [24,26], was selected as the case of study. The simulated EDBM stack was configured with 20 triplets, featuring an effective area of approximately 0.16 m^2 (34.5 cm in length, 45.4 cm in width, and 350 μm in thickness).

EDBM and PV-EDBM batch operations, lasting 9 h, were simulated using the modeling tool described in Section 2.1.

Initially, a volume of 0.600 m^3 of 1.0 $mol \cdot L^{-1}$ NaCl (as generic solution) was considered in the brine tank, while four different volumes (0.200 m^3, 0.225 m^3, 0.250 m^3, and 0.300 m^3) were studied for the base (0.05 $mol \cdot L^{-1}$ NaOH) and acid (0.05 $mol \cdot L^{-1}$ HCl) tanks, to evaluate production capacity.

The performance of the EDBM unit, powered by the electrical grid mix (constant current density) and the PV array under the solar irradiation of Lampedusa (Italy) in the months of February and August, was analyzed.

Constant current densities, with values closely aligned to those provided by the PV arrays (225–375 $A \cdot m^{-2}$), were considered for comparison of both power supplies. Additionally, a current density of 450 $A \cdot m^{-2}$ was evaluated as a reference for nominal operating conditions.

The power supply from PV solar energy was evaluated by the modeling and simulation of KC200GT (Kyocera, Japan) PV panels, whose main parameters are summarized in Table 1.

Large-scale applications typically require higher currents or voltages than those provided by an individual PV module. Therefore, this work analyzes 8 different PV array configurations (Table 2) comprising 20–33 PV panels.

Average irradiation and temperature profiles of Lampedusa in the months of February (Fig. 2.a) and August (Fig. 2.b), sourced from PV-GIS database [59], were selected. As expected, less irradiation is recorded in February in comparison to August, with maximum irradiation values of 767.7 $W \cdot m^{-2}$ and 947.7 $W \cdot m^{-2}$, respectively. Moreover, the average air temperature is lower in February (14 °C) than in August (26 °C). Furthermore, wind speed is higher in February (7.06 $m \cdot s^{-1}$) than in August (4.07 $m \cdot s^{-1}$). Operating times (shown in yellow in Fig. 2) have been set within the ranges of 7.00 h - 16.00 h (UTC) and 7.30 h - 16.30 h (UTC) for the months of February and August, respectively. This

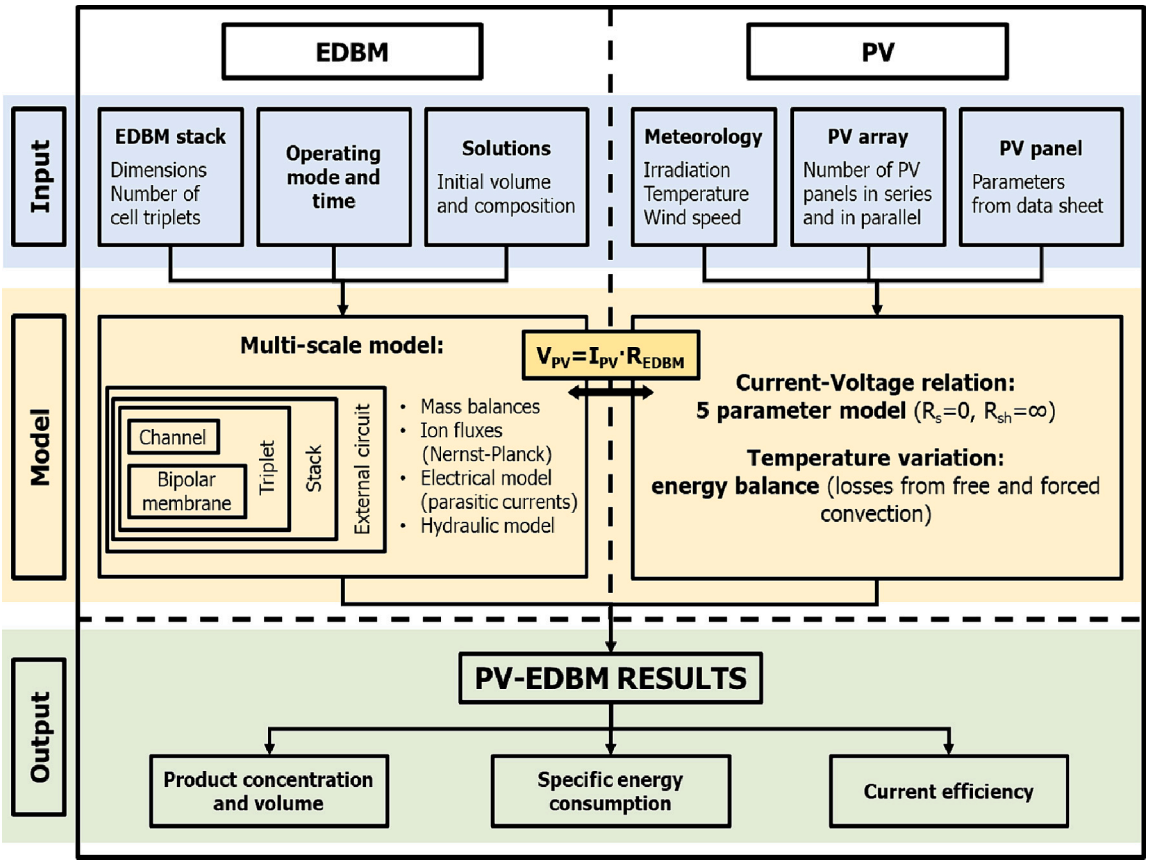

Fig. 1. PV-EDBM integrated model overview.

Table 1
KC200GT (Kyocera, Japan) PV panel parameters (from manufactures datasheet [58]).

Variable	Description	Value	Units
$I_{mp,ref}$	Maximum power point current in standard conditions	7.61	A
$I_{sc,ref}$	Short cut current in standard conditions	8.21	A
Ns	Number of cells	54	
$V_{mp,ref}$	Maximum power point voltage in standard conditions	26.3	V
$V_{oc,ref}$	Open circuit Voltage in standard conditions	32.9	V
μ_I	Temperature coefficient of I_{sc}	$3.18{\cdot}10^{-3}$	$A{\cdot}K^{-1}$
μ_V	Temperature coefficient of V_{oc}	$-1.23{\cdot}10^{-1}$	$V{\cdot}K^{-1}$
H	Height	1.425	m
W	Width	0.990	m
A	Area	1.41075	m^2

Table 2
PV array configurations.

PV Panels in parallel	10	11	12	13	8	9	10	11
PV Panels in series	2	2	2	2	3	3	3	3
Total	20	22	24	26	24	27	30	33

adjustment aims to maximize total irradiation during the 9-hour experiment.

In summary, EDBM and PV-EDBM performance under a) average current density, and b) initial acid and base volumes, has been evaluated in terms of product capacity, SEC and CE.

2.3. Economic evaluation

An economic analysis was conducted, comparing EDBM performance under the power supply provided by the electrical grid mix and the PV array. The scenarios analyzed were outlined in Section 2.2. The PV-EDBM was compared to the EDBM unit operating at a constant current density of 450 $A{\cdot}m^{-2}$. The primary aim was to calculate the Levelized Cost of NaOH (LCoNaOH, $€{\cdot}ton_{NaOH}^{-1}$), which represents the lowest sale price per ton of NaOH necessary to achieve a Net Present Value (NPV) of zero at the conclusion of the project activity (Eq. (1)).

$$LCoNaOH = \frac{Capital_{cost} + \sum_{t=1}^{n} \frac{O\&M_t + Electricity_{cost,t}}{(1+r)^t}}{\sum_{t=1}^{n} \frac{Product_{NaOH,t}}{(1+r)^t}} \quad (1)$$

where, $Capital_{cost}$ refers to the complete fixed capital investment; $O\&M_t$ signifies the annual operating and maintenance cost; $Electricity_{cost,t}$ is the cost of electricity consumed by the EDBM system; $Product_{NaOH,t}$ represents the annual produced mass of NaOH; t is the year; and r is the discount rate. The O&M cost was computed as 10 % of the total fixed capital investment. Additional parameters of the model include annual working hours, project lifespan, discount rate, and the cost of electricity (Table 3). The levelized cost calculation followed the methodology used by Lei et al. [60], where capital costs are calculated as detailed in Table 3.

The model calculates the reduction in CO_2 emissions resulting from the use of PV solar energy, as well as the economic savings attributed to the diminished carbon tax and the reduced need to purchase emission allowances from the EU ETS. Table 3 provides information on both the CO_2 emissions per kWh of energy from the grid mix and the average carbon tax and price of emission allowances from the EU ETS in 2022 (based on the EUA stock index).

3. Results and discussion

3.1. Performance comparison of energy power source: Electrical grid mix (constant current density) versus PV arrays (variable current density)

A performance comparison between two energy sources supplying the EDBM unit is presented: a) the electrical grid mix, providing constant current density; and b) the PV array, offering a variable current density.

Average current densities in the range of 279–378 $A{\cdot}m^{-2}$ for the irradiation and temperature profile of August, and 223–303 $A{\cdot}m^{-2}$ for the irradiation and temperature profile of February, have been implemented in the PV-EDBM integrated model (Table 4). As expected, the average current density value was dependent on both meteorological data (irradiation and temperature profiles, together with wind speed) and PV array configuration (number of panels and their interconnections). The results obtained under these conditions could be compared to the ones reported for constant current densities, ranging from 225 to 375 $A{\cdot}m^{-2}$, emulating a power supply from the electrical grid mix.

The variable current density profiles (Fig. 3) displayed parallelism with solar irradiation, reaching maximum values in mid-day hours (4.5 h into the simulated experiment) and minimum values at sunrise and sunset when irradiation is low (0–1 h and 8–9 h into the simulated experiment, respectively). However, as seen in Fig. 3, a limitation was detected within the PV array configurations of 2 PV panels in series

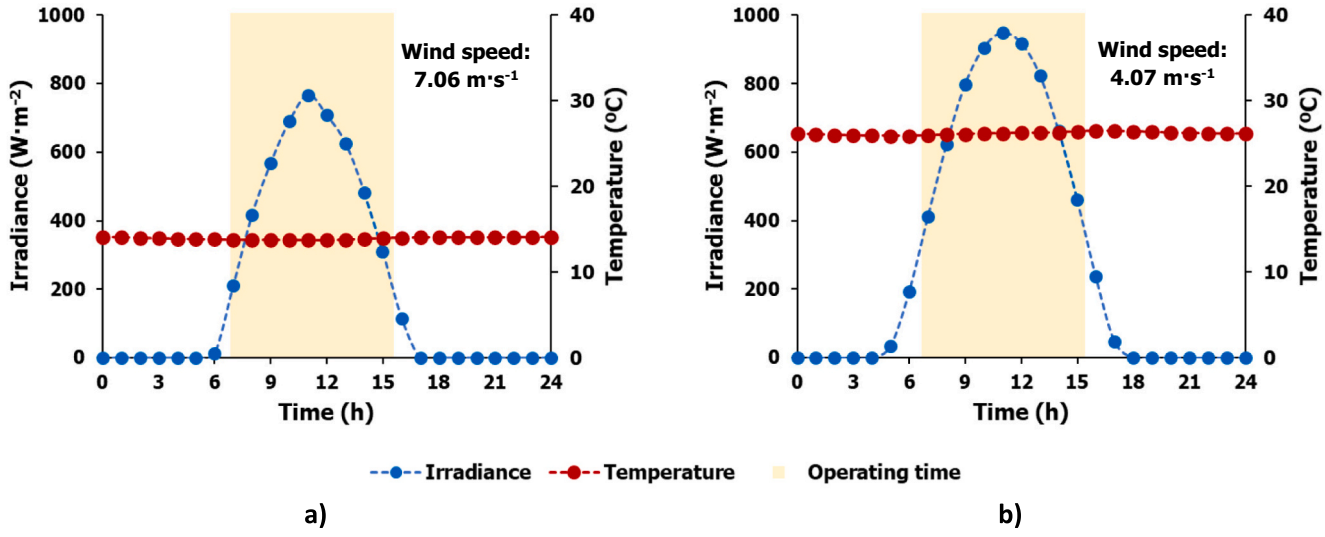

Fig. 2. Average daily irradiance and temperature profiles for Lampedusa (Italy) in a) February, and b) August.

Table 3
Input data of the economic model.

Maintenance costs			
O&M cost		Variable	0.1 × Total capital cost, [60]
Capital costs			
AEM/CEM cost	109 €·m^{-2}	120 US$·m^{-2}	[60]
BPM cost	273 €·m^{-2}	300 US$·m^{-2}	[60]
Spacer cost	9.10 €·m^{-2}	10 US$·m^{-2}	
Total cost of membranes and spacers	1670 €	1830 US$	
Cost of membrane stack	2500 €	2750 US$	1.5 × Total cost of membranes and spacer, [60]
PV panel cost	0.27 €·W^{-1}	0.3 US$·W^{-1}	
Cost of PV panels		Variable	PV panel power × PV panel cost × Number of panels
Cost of peripherals		Variable	1.5 × (Cost of membrane stack + Cost of PV panels), adapted from [60]
Total capital cost		Variable	Cost of membrane stack + Cost of PV panels + Cost of peripherals, adapted from [60]
Economic parameters			
Working hours		8000 h·y^{-1}	
Project lifetime		10 y	
Discount rate		5 %	[61]
*Electricity price	0.18 €·kWh^{-1}	0.2 US$·kWh^{-1}	[62]
CO_2 emission factor		0.294 kg CO_2·kWh^{-1}	[63]
Average Carbon Tax (EU)	44.49 €·ton^{-1} CO_2		[11]
EU ETS allowance price	**83 €·ton^{-1} CO_2		[64]

* Price of electricity set based on European statistics for non-household consumers.
** Average EU ETS price. September 2023.

during the central hours because the maximum voltage value of the PV array was reached, placing the operating point of the PV array at a low intensity value. This limitation was more pronounced in the case of the irradiation and temperature profile of August (Fig. 3.a) compared to the February profile (Fig. 3.b), particularly between 1.5 and 7.5 h approx. and 2.5–6.5 h approx., respectively. Thus, PV array configurations of 3 PV panels in series should be selected in this case of study in order to avoid this constraint.

Fig. 4 depicts the evolution of NaOH concentration in the base solution through the simulated experiments. NaOH was chosen as the target product due to its higher market prices and requirements in industrial facilities, such as desalination plants, compared to HCl [34]. Nevertheless, equivalent performances were observed for both NaOH and HCl.

NaOH concentration increased with time when EDBM, operated with a constant current density, was simulated (Fig. 4.a). However, this performance was not linear as the EDBM model considered non-ideal phenomena [27], fitting to the real performance of the process. As expected from previous works [23], higher NaOH concentrations were achieved when higher current densities were applied. The production of 0.25 m^3 of 1.0 mol·L^{-1} NaOH was achieved for a minimum current density of 300 A·m^{-2}. Therefore, if lower or higher current densities are employed, smaller or grater volumes of NaOH at the same concentration would be produced, respectively.

The same NaOH concentrations at the end of the simulated experiment (9 h) were obtained for the same value of average current density, regardless of constant or variable profile. For instance, 0.25 m^3 of ~1.0 mol·L^{-1} NaOH were produced under 300 A·m^{-2} (constant), a PV array with a PV panel configuration of 12 in parallel and 2 in series and an irradiation and temperature profiles of August (average of 303 A·m^{-2}), and a PV array with a PV panel configuration of 11 in parallel and 3 in series and an irradiation and temperature profiles of February (average of 303 A·m^{-2}). As for constant current densities, higher NaOH concentrations were achieved with higher average current densities under variable profiles. In this sense, higher concentrations were obtained using the irradiation and temperature profiles of August (Fig. 4.b) compared to those in February (Fig. 4.c) for the same PV array. The main difference in performance, which was observed when operating with PV arrays, was the sigmoidal shape of the NaOH concentration curve. This means that larger variations in the NaOH concentration were obtained in the middle of the simulated experiment, corresponding to the maximum values of the current density, in contrast to the initial and final values (minimums in current densities). These sigmoidal shapes were also reported in experimental PV-EDBM previous works [23]. The same performance was observed for the evolution of NaOH volume (Fig. 5).

Figs. 6 and 7 depict SEC and CE evolution in the different simulations, respectively. SEC measures the energy consumed by the EDBM in generating 1 kg of product, whereas CE relates the equivalent charge transported across ion exchange membranes (product generation) with the electric current applied.

SEC increased over time during simulations at constant current density (Fig. 6.a), as the energy supplied to the EDBM remained approximately constant, but the variation in NaOH concentration was not linear due to non-ideal phenomena involved in the process, such as ion back diffusion (due to concentration gradient) or water transport (osmotic pressure difference).

On the other hand, SEC increased until it reached a plateau when simulating variable current density (Fig. 6.b and c) because, in addition to the variable energy consumed over time, these simulations reported a sigmoidal evolution of NaOH concentration. The plateau value was higher for higher current densities (Fig. 6.b and c, individually) and when comparing the results between the profiles of August and February (comparison between Fig. 6.b and c), with the former values being

Table 4
Average current densities for the 8 PV arrays analyzed considering irradiation and temperature profiles of August and February in Lampedusa (Italy).

PV array (number of panels)			Average current density (A·m^{-2})	
Parallel	Series	Total	August - Lampedusa	February - Lampedusa
10	2	20	279	253
11	2	22	292	271
12	2	24	303	287
13	2	26	313	302
8	3	24	292	223
9	3	27	323	250
10	3	30	351	277
11	3	33	378	303

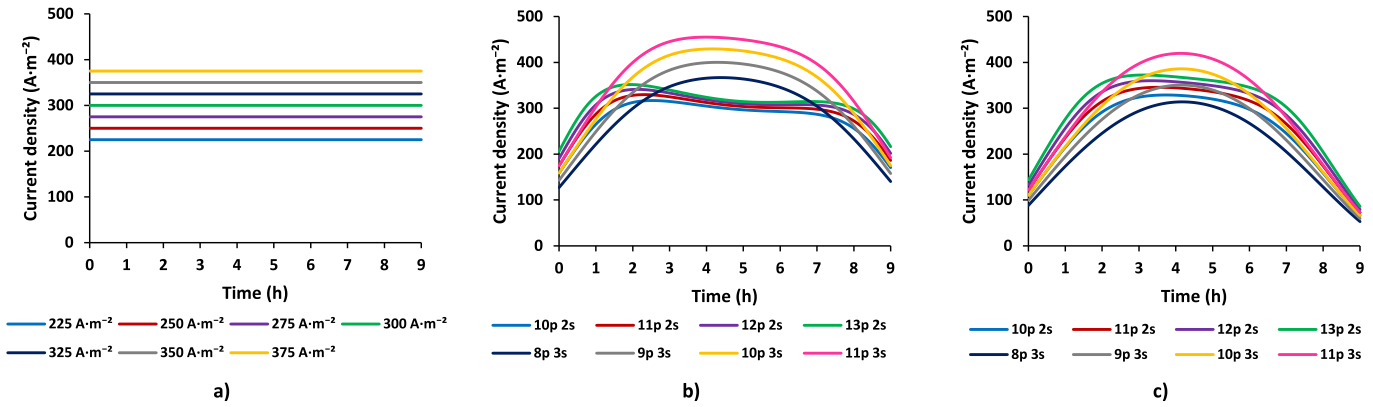

Fig. 3. Evolution of current density: a) electrical grid mix (the same range than the ones obtained for PV-EDBM, for comparison purposes), b) PV array - Lampedusa August (from 7.30 to 16.30 UTC), and c) PV array - Lampedusa February (from 7.00 to 16.00 UTC). Initial NaOH volume of 0.25 m^3.

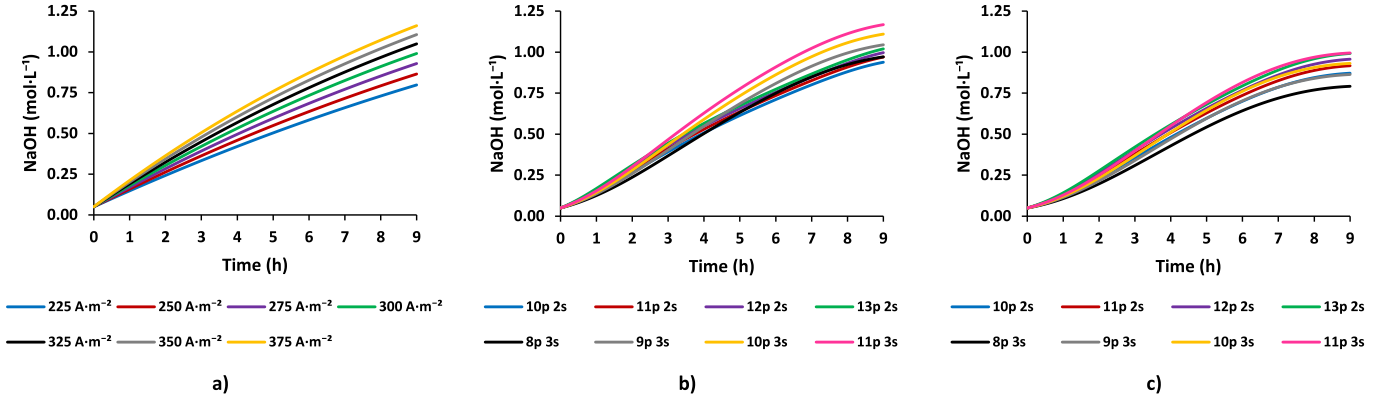

Fig. 4. Evolution of NaOH concentration: a) electrical grid mix, b) PV array - Lampedusa August, and c) PV array - Lampedusa February. Initial NaOH volume of 0.25 m^3.

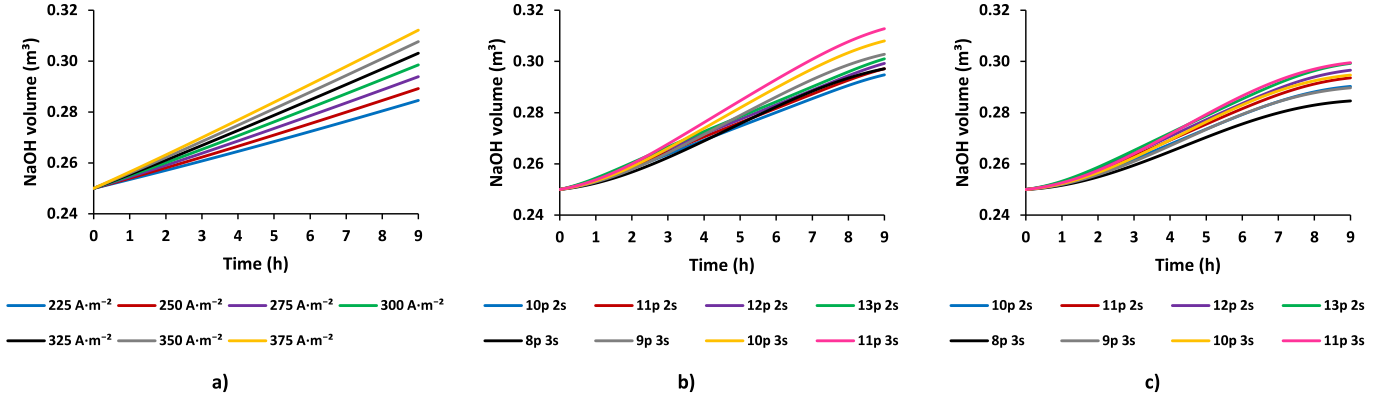

Fig. 5. Evolution of NaOH volume: a) electrical grid mix, b) PV array - Lampedusa August (from 7.30 to 16.30 UTC), and c) PV array - Lampedusa February (from 7.00 to 16.00 UTC). Initial NaOH volume of 0.25 m^3.

higher.

PV array configurations of 2 PV panels in series reached the SEC plateau value in a shorter time due to the PV array maximum voltage limitation. This fact is more noticeable when irradiation and temperature profiles of summer were selected (Fig. 6.b).

It is worth noting that the SEC values of the PV array configurations of 3 PV panels in series under the irradiation and temperature profiles of February at the end of the simulated experiment were slightly below the plateau, due to them having especially low current densities. This reduced the value of the energy provided, without affecting the production of NaOH in the same way (Fig. 6.c).

Moreover, the CE had a decreasing trend (Fig. 7) and, therefore, opposed the SEC. CE decreased over time during simulations at constant current density (Fig. 7.a). Initially, higher CE values were reported for higher current densities, whereas the end CE values were lower for the higher current density values.

This suggests a higher drop in the performance over time for the higher current densities, probably because the impact of non-ideal phenomena increases when products concentrations rise [26].

The main difference observed when operating with PV arrays (Fig. 7.

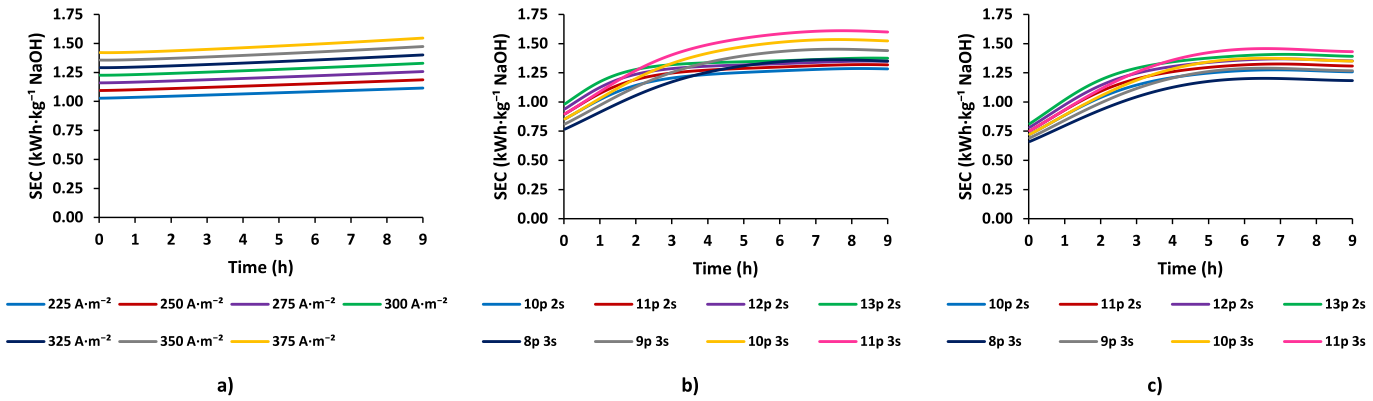

Fig. 6. Evolution of SEC: a) electrical grid mix, b) PV array - Lampedusa August (from 7.30 to 16.30 UTC), and c) PV array - Lampedusa February (from 7.00 to 116.00 UTC). Initial NaOH volume of 0.25 m^3.

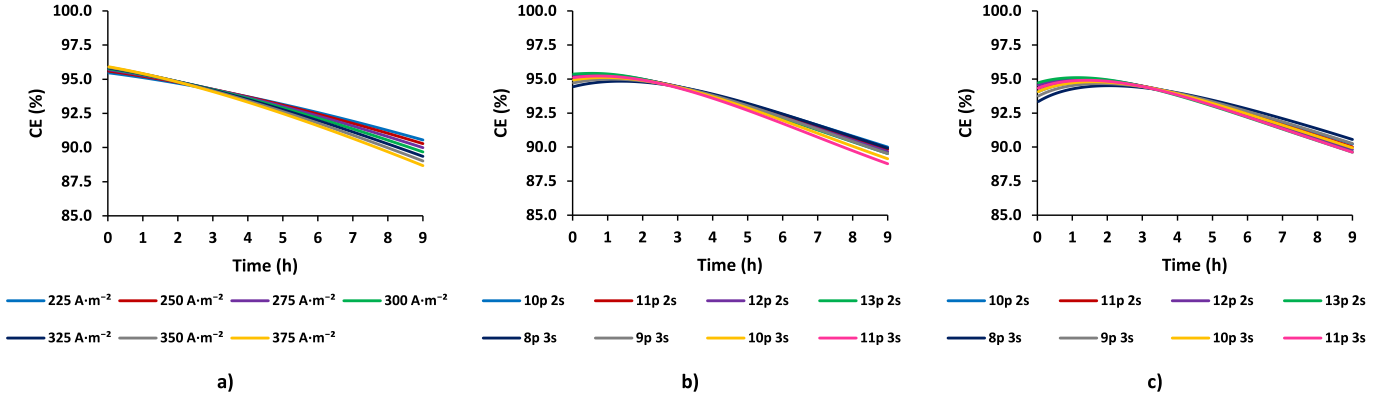

Fig. 7. Evolution of CE: a) electrical grid mix, b) PV array - Lampedusa August (from 7.30 to 16.30 UTC), and c) PV array - Lampedusa February (from 7.00 to 16.00 UTC). Initial NaOH volume of 0.25 m^3.

b and c) was that CE increased initially until it reached a maximum and then decreased, for all the average current densities. This pattern is related to the low initial current densities that could favor diffusion across the membranes against the electrical gradient (non-ideal phenomenon). In fact, it is more noticeable for irradiation and temperatures profiles of February (Fig. 7.c) than for irradiation and temperatures profiles of August (Fig. 7.b).

3.2. Evaluation of production capacity (products volumes) under the current density provided by electrical grid mix and PV arrays

The installation of a specific PV array configuration introduces variability in the average current density, as it is highly dependent on weather conditions and seasonality. Achieving higher average current densities would allow generating more concentrated products or larger volumes at a given concentration. In this section, the production capacity (referring to the initial volume of NaOH, 0.2–0.3 m^3, at the same initial concentration of 0.05 $mol \cdot L^{-1}$) under three energy power sources is analyzed (Fig. 8): a) electrical grid mix, with a constant current density of 450 $A \cdot m^{-2}$ (considered as maximum); b) PV array configured with 11 PV modules in parallel and 3 PV modules in series under irradiation and temperature profiles of August (average current density of 378 $A \cdot m^{-2}$ and maximum current density of 455 $A \cdot m^{-2}$); and c) PV array configured with 11 PV modules in parallel and 3 PV modules in series under irradiation and temperature profiles of February (average current density of 303 $A \cdot m^{-2}$ and maximum current density of 420 $A \cdot m^{-2}$).

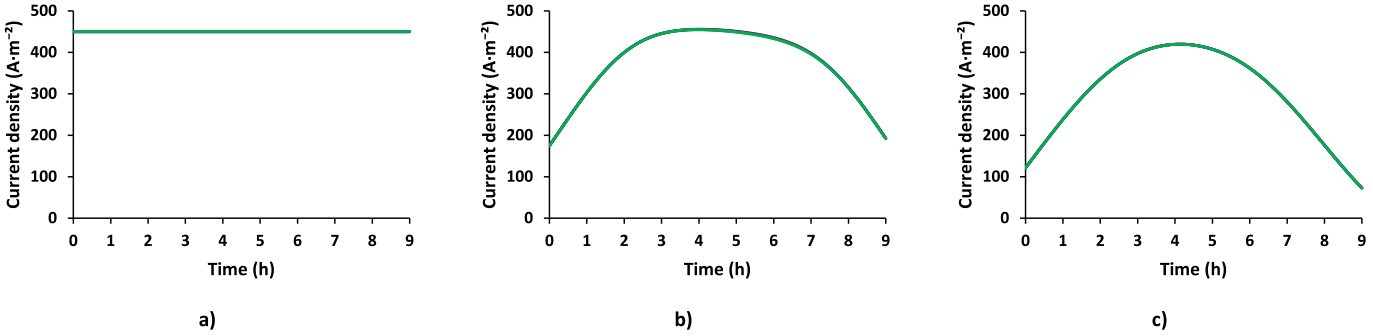

Fig. 8. Initial NaOH volume analysis. Evolution of current density: a) 450 $A \cdot m^{-2}$ supplied by electrical grid mix, b) PV array (11 in parallel and 3 in series) - Lampedusa August (from 7.30 to 16.30 UTC), and c) PV array (11 in parallel and 3 in series) - Lampedusa February (from 7.00 to 16.00 UTC). Current density profiles are independent from initial NaOH volumes.

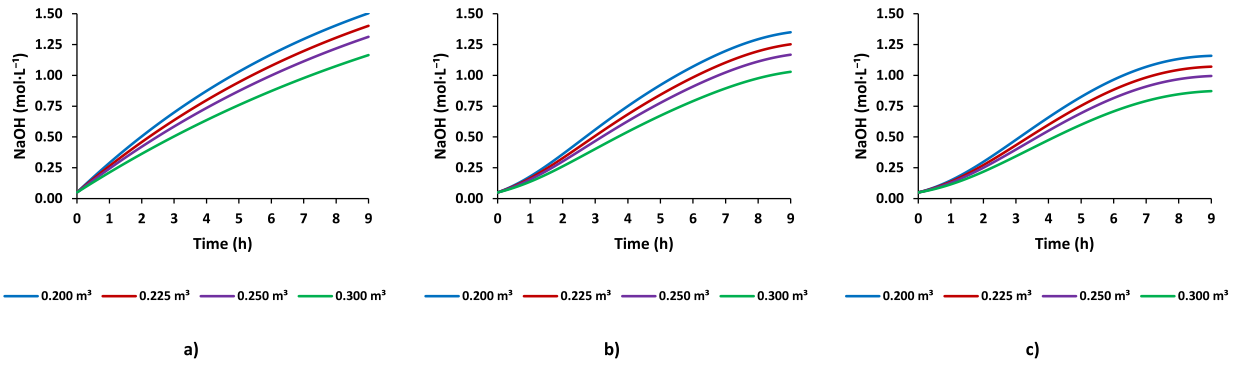

Fig. 9. Initial NaOH volume analysis. Evolution of NaOH concentration: a) 450 A·m^{-2} supplied by electrical grid mix, b) PV array (11 in parallel and 3 in series) - Lampedusa August (from 7.30 to 16.30 UTC), and c) PV array (11 in parallel and 3 in series) - Lampedusa February (from 7.00 to 16.00 UTC).

As seen in Fig. 9, higher NaOH concentrations were obtained when higher average current densities were applied. Moreover, larger initial volumes led to lower final product concentrations. If 1.0 mol·L^{-1} NaOH is fixed as a target, working under constant current density (450 A·m^{-2}) reduces operating time to 5–7 h for 0.2–0.3 m^3, respectively (Fig. 9.a). Whereas 5.5–8 h are required for 0.2–0.3 m^3 under the profiles of August in Lampedusa (Fig. 9.b) and 6–9 h are required for 0.2–0.25 m^3 under the profiles of February in Lampedusa (Fig. 9.c), not being able to achieve the target for 0.3 m^3 throughout the operating day (9 h).

Volumes increased with time due to the electro-osmotic transportation of water across the membranes, therefore, dependent on the current density. Thus, a parallel evolution of volumes was observed under the same current density profile (Fig. 10). It is obvious that a larger initial volume leads to a larger end volume.

Initial volume variations in the range of 0.2–0.3 m^3 did not significantly modify the SEC under the same current density profile (Fig. 11). Despite the fact that higher concentrations could be achieved at the same operating time (or same concentrations at a lower operating time), working at a constant current density of 450 A·m^{-2} reported higher SEC than operating with the PV array in both August and February in Lampedusa, irradiance and temperature profiles. Hence, if operating times or final concentrations are not considered a limitation, the use of a PV array could reduce the SEC of EDBM, promoting the environmental sustainability of the process due to a reduction in the indirect emissions through the use of renewable energy.

Fig. 12 depicts a decreasing trend in CE as product concentrations are increased, due to concentration polarization (a non-ideal phenomenon). Therefore, lower CE was reported for lower initial NaOH volumes, as higher product concentrations were achieved for the same operating time and current density profile.

3.3. Techno-economic analysis

This section presents an economic comparison between EDBM powered by the electrical grid mix and PV solar energy, considering seasonal variations, current density, and array configurations detailed in Section 3.2. The selected PV array configuration had 3 panels in series and 11 panels in parallel, striking a balance between energy efficiency and potential capital expenditure. The PV-EDBM with variable current was compared to the grid mix with a constant current density (450 A·m^{-2}). Fig. 13 displays a histogram that reports the overall LCoNaOH and all the relevant contributions to LCoNaOH, for both EDBM and PV-EDBM (considering the variability through the year).

The EDBM operated with the grid mix showed a LCoNaOH of 254 €·ton^{-1} NaOH. Conversely, although the use of PV solar energy increases capital and O&M costs, these costs are offset by the fact that electricity does not have to be purchased from the grid mix. Therefore, using PV solar energy results in an overall reduction of 7.3 % in the LCoNaOH in February and 33 % in August. The lesser advantage in the month of February is clearly related to the reduced solar irradiation. Overall, during the solar year, the LCoNaOH drops by an average of 20 % compared to grid mix.

The breakdown cost analysis in Fig. 13 reveals that when the EDBM is powered by the grid mix, the major influencing factor on the LCoNaOH is the cost of electricity, accounting for 65 % of the LCoNaOH. Notably, this electricity cost becomes zero when switching to PV solar energy. However, the levelized cost contributions of factors related to peripherals and O&M costs are higher with PV solar energy than grid mix energy. Although the contribution of membranes, spacers, and stack frame to the LCoNaOH varies across the scenarios due to slight variations in productivity, the unit costs for the membranes, spacers, and stack frame remain constant across all scenarios. This indicates that the

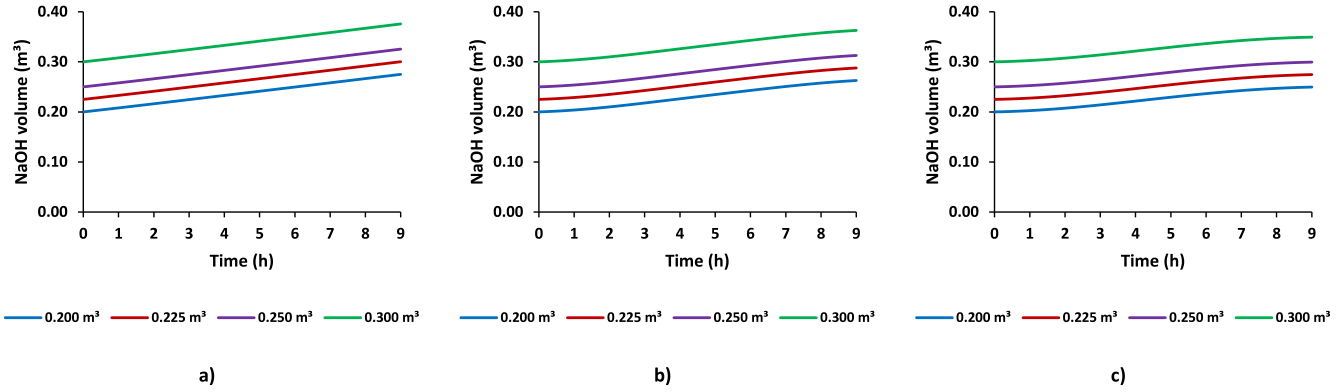

Fig. 10. Initial NaOH volume analysis. Evolution of NaOH volume: a) 450 A·m^{-2} supplied by electrical grid mix, b) PV array (11 in parallel and 3 in series) - Lampedusa August (from 7.30 to 16.30 UTC), and c) PV array (11 in parallel and 3 in series) - Lampedusa February (from 7.00 to 16.00 UTC).

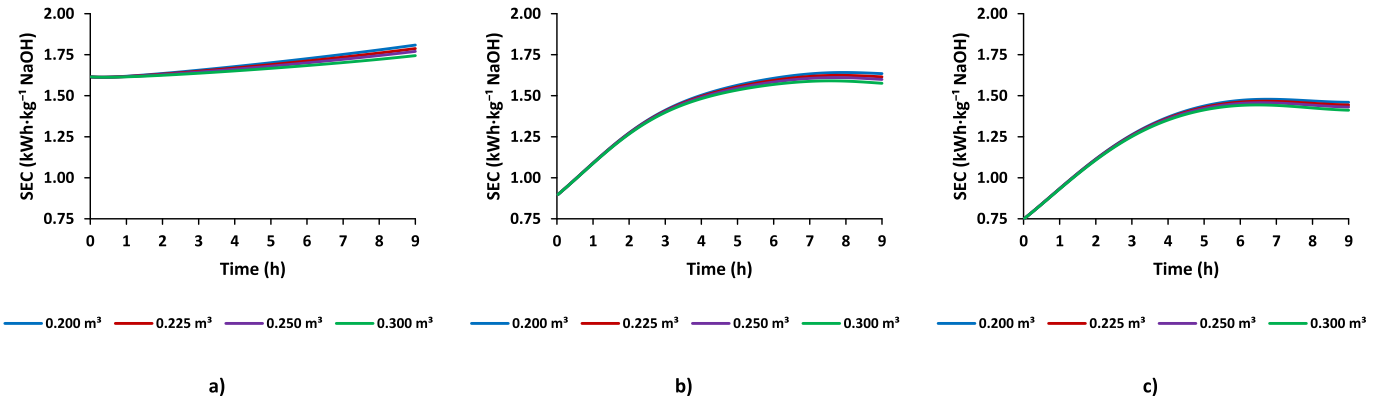

Fig. 11. Initial NaOH volume analysis. Evolution of specific energy consumption: a) 450 A·m^{-2} supplied by electrical grid mix, b) PV array (11 in parallel and 3 in series) - Lampedusa August (from 7.30 to 16.30 UTC), and c) PV array (11 in parallel and 3 in series) - Lampedusa February (from 7.00 to 16.00 UTC).

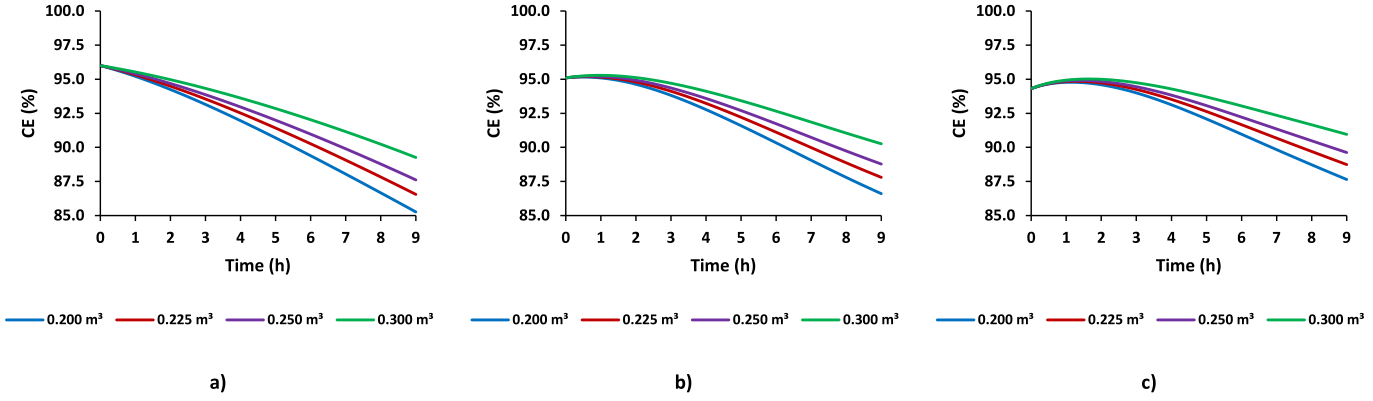

Fig. 12. Initial NaOH volume analysis. Evolution of current efficiency: a) 450 A·m^{-2} supplied by electrical grid mix, b) PV array (11 in parallel and 3 in series) - Lampedusa August (from 7.30 to 16.30 UTC), and c) PV array (11 in parallel and 3 in series) - Lampedusa February (from 7.00 to 16.00 UTC).

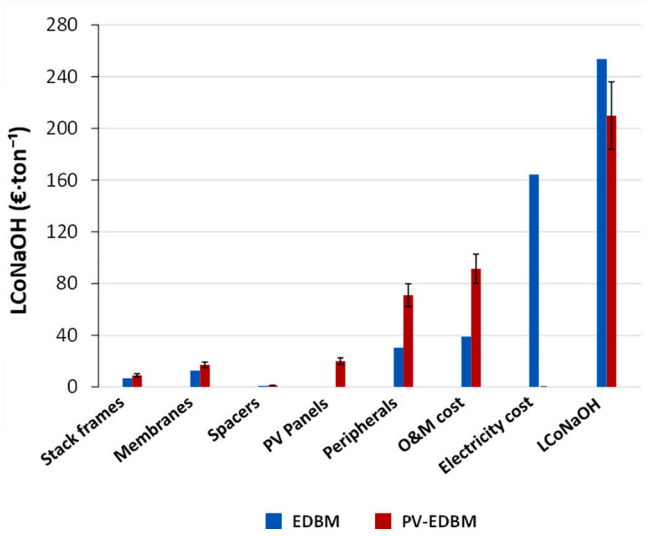

Fig. 13. Comparison of LCoNaOH in an exploded view for both grid mix and PV solar energy (yearly average), in Lampedusa (Italy). Black bars represent seasonal variability of costs from February (maximum value) to August (minimum value).

differences in their contributions to the levelized cost are not due to changes in their individual prices, which are identical for the equipment under study, but rather to how their relative impact on the levelized cost shifts between scenarios. The costs of stack frames, membranes, and spacers do not significantly impact the levelized cost, accounting for about 8–13 %. A decrease in these costs, especially the membranes, could indirectly lead to a considerable reduction in peripheral and O&M costs.

According to the results, capital costs of PV-EDBM (e.g., for the acquisition of PV panels) are more relevant than operating costs. In contrast, the opposite is true when using the electrical grid mix. Based on the LCoNaOH comparisons, for NaOH production, the utilization of PV-EDBM units can significantly lower the overall LCoNaOH. These conclusions may be applied to the case of hydrochloric acid production due to the similarity in the HCl productivity. Taken together, the PV-EDBM can produce NaOH and HCl at prices that are competitive with current market prices. Besides, another advantage of PV solar energy is the almost zero emissions of GHG, such as CO_2. In comparison, using the electrical grid mix in the investigated scenarios would result in emissions in the order of 0.53 kg CO_2·kg^{-1} NaOH. The energy consumed when using the grid mix to power the EDBM in this study would lead to a carbon tax of 23.6 €·ton^{-1} NaOH and an emissions allowance cost of 44.1 €·ton^{-1} NaOH.

4. Conclusions

This study introduces a novel integrated model of photovoltaic solar electrodialysis with bipolar membranes (PV-EDBM) which has been developed and thoroughly assessed. This model proves to be a valuable tool for the evaluation and sizing of EDBM facilities powered by renewable energies, specifically PV solar.

The integrated model has been applied to assess the techno-

economic feasibility of a potential PV-EDBM plant dedicated to the production of NaOH and HCl from brines, and which is located in the SWRO facility of the island of Lampedusa (Italy), powered either by the electrical grid mix or a PV array.

The transition from the electrical grid mix (constant current density) to PV solar (variable current density) resulted in a comparable performance in terms of product concentration, SEC and CE, as long as the same average current densities were employed. However, the utilization of PV solar energy entails the application of current densities that may exceed supplier recommendations during peak daylight hours, potentially impacting membrane lifespan. Conversely, the constraints of current density with the grid mix may prevent full exploitation of maximum capacity in the EDBM plant.

The economic analysis revealed that the LCoNaOH of the PV-EDBM integrated process was lower because the extra cost of constructing the PV panels was offset by the elimination of the electricity cost from the grid mix. Furthermore, the adoption of PV-EDBM significantly reduces emissions, which in turn lowers the costs associated with the carbon tax and EU ETS allowances.

Overall, the integration of PV solar energy with EDBM emerges as an economically feasible investment, enhancing the viability of EDBM as a technology for resource recovery.

Consequently, the findings presented herein contribute to advancing the integration of renewable energies with electro-membrane technologies, exemplified by EDBM, and they underscore the great potential of renewable energies in the decarbonization of industrial processes.

Funding sources

Grant TED2021-129874B-I00 funded by MCIN/AEI/ 10.13039/501100011033 and by the “European Union NextGenerationEU/PRTR”.

M. Herrero-Gonzalez research was developed under the Margarita Salas postdoctoral fellowship from Ministerio de Universidades (MIU, Spain) and funded by the European Union–NextGenerationEU.

CRediT authorship contribution statement

Marta Herrero-Gonzalez: Conceptualization, Methodology, Software, Validation, Formal analysis, Investigation, Writing - Original Draft, Visualization. **Andrea Culcasi:** Methodology, Software, Validation, Formal analysis, Investigation, Writing - Original Draft. **Alessandro Tamburini:** Writing - review & editing, Supervision. **Raquel Ibañez:** Conceptualization, resources, Writing - review & editing, Supervision, Funding acquisition. **Andrea Cipollina:** Conceptualization, resources, Writing - review & editing, Supervision, Funding acquisition. **Giorgio Micale:** Supervision.

Declaration of competing interest

The authors declare that they have no known competing financial interests or personal relationships that could have appeared to influence the work reported in this paper.

Data availability

Data will be made available on request.

References

[1] United Nations, Home - United Nations Sustainable Development Goals. https://www.un.org/sustainabledevelopment/, 2023. (Accessed 8 May 2023).
[2] European Commission, A European Green Deal, European Commission, 2023. https://ec.europa.eu/info/strategy/priorities-2019-2024/european-green-deal_en. (Accessed 8 May 2023).
[3] S. Bobba, S. Carrara, J. Huisman, F. Mathieux, C. Pavel, Critical Raw Materials for Strategic Technologies and Sectors in the EU - A Foresight Study, Publications Office of the European Union, 2020, https://doi.org/10.2873/58081.
[4] H. Chen, H. Wu, N.S.A. Khan, X. Peng, F. Qiu, T. Zhang, Converting wastes to resource: preparation of NiO@γ-Al2O3 sludge composite from aluminum-containing sludge for cadmium removal from wastewater, J. Clean. Prod. 392 (2023) 136335, https://doi.org/10.1016/j.jclepro.2023.136335.
[5] L.F. Petrik, H.H. Ngo, S. Varjani, P. Osseweijer, D. Xevgenos, M. van Loosdrecht, M. Smol, X. Yang, J. Mateo-Sagasta, From wastewater to resource, One Earth 5 (2022) 122–125, https://doi.org/10.1016/j.oneear.2022.01.011.
[6] V.S.C. Tunn, N.M.P. Bocken, E.A. van den Hende, J.P.L. Schoormans, Business models for sustainable consumption in the circular economy: an expert study, J. Clean. Prod. 212 (2019) 324–333, https://doi.org/10.1016/j.jclepro.2018.11.290.
[7] I. Ihsanullah, J. Mustafa, A.M. Zafar, M. Obaid, M.A. Atieh, N. Ghaffour, Waste to wealth: a critical analysis of resource recovery from desalination brine, Desalination 543 (2022) 116093, https://doi.org/10.1016/j.desal.2022.116093.
[8] E. Fernández-Escalante, R. Ibañez, Ma.-F. San-Román, Selective lithium separation from desalination concentrates via the synergy of extractant mixtures, Desalination 556 (2023) 116525, https://doi.org/10.1016/j.desal.2023.116525.
[9] S. Sharma, S. Basu, N.P. Shetti, T.M. Aminabhavi, Waste-to-energy nexus for circular economy and environmental protection: recent trends in hydrogen energy, Sci. Total Environ. 713 (2020) 136633, https://doi.org/10.1016/j.scitotenv.2020.136633.
[10] European ComissionCommission, EU Emissions Trading System (EU ETS), European Commission, 2023. https://climate.ec.europa.eu/eu-action/eu-emissions-trading-system-eu-ets_en (accessed October 3, 2023).
[11] Tax Fundation, Carbon Taxes in Europe, Tax Fundation, 2023. https://taxfoundation.org/data/all/eu/carbon-taxes-in-europe-2023/. (Accessed 3 October 2023).
[12] A. Prado de Nicolás, A. Molina-García, J.T. García-Bermejo, F. Vera-García, Reject brine management: denitrification and zero liquid discharge (ZLD)—current status, challenges and future prospects, J. Clean. Prod. 381 (2022) 135124, https://doi.org/10.1016/j.jclepro.2022.135124.
[13] Y. Liu, X. Wu, X. Wu, L. Dai, J. Ding, X. Ye, R. Chen, R. Ding, J. Liu, Y. Jin, B. Van der Bruggen, Recovery of nickel, phosphorus and nitrogen from electroless nickel-plating wastewater using bipolar membrane electrodialysis, J. Clean. Prod. 382 (2023) 135326, https://doi.org/10.1016/j.jclepro.2022.135326.
[14] L. Gurreri, A. Tamburini, A. Cipollina, G. Micale, Electrodialysis applications in wastewater treatment for environmental protection and resources recovery: a systematic review on progress and perspectives, Membranes (Basel) 10 (2020) 146, https://doi.org/10.3390/membranes10070146.
[15] J.-M. Arana Juve, F.M.S. Christensen, Y. Wang, Z. Wei, Electrodialysis for metal removal and recovery: a review, Chem. Eng. J. 435 (2022) 134857, https://doi.org/10.1016/j.cej.2022.134857.
[16] R. Pärnamäe, S. Mareev, V. Nikonenko, S. Melnikov, N. Sheldeshov, V. Zabolotskii, H.V.M. Hamelers, M. Tedesco, Bipolar membranes: a review on principles, latest developments, and applications, J. Membr. Sci. 617 (2021) 118538, https://doi.org/10.1016/j.memsci.2020.118538.
[17] C. Fernandez-Gonzalez, A. Dominguez-Ramos, R. Ibañez, A. Irabien, Electrodialysis with bipolar membranes for valorization of brines, Sep. Purif. Rev. 45 (2016) 275–287, https://doi.org/10.1080/15422119.2015.1128951.
[18] M. Reig, S. Casas, C. Valderrama, O. Gibert, J.L. Cortina, Integration of monopolar and bipolar electrodialysis for valorization of seawater reverse osmosis desalination brines: production of strong acid and base, Desalination 398 (2016) 87–97, https://doi.org/10.1016/j.desal.2016.07.024.
[19] A. Kumar, K.R. Phillips, J. Cai, U. Schröder, J.H. Lienhard, Integrated valorization of desalination brine through NaOH recovery: opportunities and challenges, Angew. Chem. Int. Ed. 58 (2019) 6502–6511, https://doi.org/10.1002/anie.201810469.
[20] M. Herrero-Gonzalez, R. Ibañez, Chemical and energy recovery alternatives in SWRO desalination through electro-membrane technologies, Appl. Sci. 11 (2021) 8100, https://doi.org/10.3390/app11178100.
[21] C. Morgante, F. Vassallo, D. Xevgenos, A. Cipollina, M. Micari, A. Tamburini, G. Micale, Valorisation of SWRO brines in a remote island through a circular approach: techno-economic analysis and perspectives, Desalination 542 (2022) 116005, https://doi.org/10.1016/j.desal.2022.116005.
[22] T. León, S. Abdullah Shah, J. López, A. Culcasi, L. Jofre, A. Cipollina, J.L. Cortina, A. Tamburini, G. Micale, Electrodialysis with bipolar membranes for the generation of NaOH and HCl solutions from brines: an inter-laboratory evaluation of thin and ultrathin non-woven cloth-based ion-exchange membranes, Membranes (Basel) 12 (2022) 1204, https://doi.org/10.3390/membranes12121204.
[23] M. Herrero-Gonzalez, P. Díaz-Guridi, A. Dominguez-Ramos, A. Irabien, R. Ibañez, Highly concentrated HCl and NaOH from brines using electrodialysis with bipolar membranes, Sep. Purif. Technol. 242 (2020) 116785, https://doi.org/10.1016/j.seppur.2020.116785.
[24] C. Cassaro, G. Virruso, A. Culcasi, A. Cipollina, A. Tamburini, G. Micale, Electrodialysis with bipolar membranes for the sustainable production of chemicals from seawater brines at pilot plant scale, ACS Sustain. Chem. Eng. 11 (2023) 2989–3000.
[25] L. Gazigil, E. Er, O.E. Kestioğlu, T. Yonar, Pilot-scale test results of electrodialysis bipolar membrane for reverse-osmosis concentrate recovery, Membranes (Basel) 12 (2022) 83, https://doi.org/10.3390/membranes12010083.
[26] M. Herrero-Gonzalez, J. López, G. Virruso, C. Cassaro, A. Tamburini, A. Cipollina, J.L. Cortina, R. Ibañez, G. Micale, Analysis of operational parameters in acid and base production using an electrodialysis with bipolar membranes pilot plant, Membranes (Basel) 13 (2023) 200, https://doi.org/10.3390/membranes13020200.

[27] A. Culcasi, L. Gurreri, A. Cipollina, A. Tamburini, G. Micale, A comprehensive multi-scale model for bipolar membrane electrodialysis (BMED), Chem. Eng. J. 437 (2022) 135317, https://doi.org/10.1016/j.cej.2022.135317.
[28] M. Mier, R. Ibañez, I. Otiz, Influence of ion concentration on the kinetics of electrodialysis with bipolar membranes, Sep. Purif. Technol. 59 (2008) 197–205, https://doi.org/10.1016/j.seppur.2007.06.015.
[29] S. Koter, A. Warszawski, A new model for characterization of bipolar membrane electrodialysis of brine, Desalination 198 (2006) 111–123, https://doi.org/10.1016/j.desal.2006.09.016.
[30] L. Shi, Y. Hu, S. Xie, G. Wu, Z. Hu, X. Zhan, Recovery of nutrients and volatile fatty acids from pig manure hydrolysate using two-stage bipolar membrane electrodialysis, Chem. Eng. J. 334 (2018) 134–142, https://doi.org/10.1016/j.cej.2017.10.010.
[31] Y. Luo, Y. Liu, J. Shen, B. Van der Bruggen, Application of bipolar membrane electrodialysis in environmental protection and resource recovery: a review, Membranes (Basel) 12 (2022) 829, https://doi.org/10.3390/membranes12090829.
[32] A. Culcasi, L. Gurreri, A. Tamburini, A. Cipollina, I.D.L. Bogle, G. Micale, Improving efficiency and discharge power of acid-base flow battery via a bi-objective optimisation, J. Energy Storage 66 (2023) 107429, https://doi.org/10.1016/j.est.2023.107429.
[33] Y. Yang, X. Gao, A. Fan, L. Fu, C. Gao, An innovative beneficial reuse of seawater concentrate using bipolar membrane electrodialysis, J. Membr. Sci. 449 (2014) 119–126, https://doi.org/10.1016/j.memsci.2013.07.066.
[34] M. Herrero-Gonzalez, R. Ibañez, Technical and environmental feasibilities of the commercial production of NaOH from brine by means of an integrated EDBM and evaporation process, Membranes (Basel) 12 (2022) 885, https://doi.org/10.3390/membranes12090885.
[35] E.T. Sayed, A.G. Olabi, K. Elsaid, M. Al Radi, R. Alqadi, M. Ali Abdelkareem, Recent progress in renewable energy based-desalination in the Middle East and North Africa MENA region, J. Adv. Res. (2022), https://doi.org/10.1016/j.jare.2022.08.016.
[36] M.K. Shahid, B. Mainali, P.R. Rout, J.W. Lim, M. Aslam, A.E. Al-Rawajfeh, Y. Choi, A review of membrane-based desalination systems powered by renewable energy sources, Water (Basel) 15 (2023) 534, https://doi.org/10.3390/w15030534.
[37] N. Mir, Y. Bicer, Integration of electrodialysis with renewable energy sources for sustainable freshwater production: a review, J. Environ. Manag. 289 (2021) 112496, https://doi.org/10.1016/j.jenvman.2021.112496.
[38] C. Fernandez-Gonzalez, A. Dominguez-Ramos, R. Ibañez, A. Irabien, Sustainability assessment of electrodialysis powered by photovoltaic solar energy for freshwater production, Renew. Sust. Energ. Rev. 47 (2015) 604–615, https://doi.org/10.1016/j.rser.2015.03.018.
[39] S. Gorjian, B. Ghobadian, H. Ebadi, F. Ketabchi, S. Khanmohammadi, Applications of solar PV systems in desalination technologies, in: Photovoltaic Solar Energy Conversion, Elsevier, 2020, pp. 237–274, https://doi.org/10.1016/B978-0-12-819610-6.00008-9.
[40] J.M. Ortiz, E. Expósito, F. Gallud, V. García-García, V. Montiel, A. Aldaz, Desalination of underground brackish waters using an electrodialysis system powered directly by photovoltaic energy, Sol. Energy Mater. Sol. Cells 92 (2008) 1677–1688, https://doi.org/10.1016/J.SOLMAT.2008.07.020.
[41] A. Gonzalez, M. Grágeda, S. Ushak, Assessment of pilot-scale water purification module with electrodialysis technology and solar energy, Appl. Energy 206 (2017) 1643–1652, https://doi.org/10.1016/j.apenergy.2017.09.101.
[42] J.M.M. Ortiz, E. Expósito, F. Gallud, V. García-García, V. Montiel, A. Aldaz, Photovoltaic electrodialysis system for brackish water desalination: modeling of global process, J. Membr. Sci. 274 (2006) 138–149, https://doi.org/10.1016/j.memsci.2005.08.006.
[43] A. Campione, A. Cipollina, F. Calise, A. Tamburini, M. Galluzzo, G. Micale, Coupling electrodialysis desalination with photovoltaic and wind energy systems for energy storage: dynamic simulations and control strategy, Energy Convers. Manag. 216 (2020) 112940, https://doi.org/10.1016/j.enconman.2020.112940.
[44] H. Xu, X. Ji, L. Wang, J. Huang, J. Han, Y. Wang, Performance study on a small-scale photovoltaic electrodialysis system for desalination, Renew. Energy 154 (2020) 1008–1013, https://doi.org/10.1016/j.renene.2020.03.066.
[45] M. Herrero-Gonzalez, P. Diaz-Guridi, A. Dominguez-Ramos, R. Ibañez, A. Irabien, Photovoltaic solar electrodialysis with bipolar membranes, Desalination 433 (2018) 155–163, https://doi.org/10.1016/j.desal.2018.01.015.
[46] M. Herrero-Gonzalez, A. Wolfson, A. Dominguez-Ramos, R. Ibañez, A. Irabien, Monetizing environmental footprints: index development and application to a solar-powered chemicals self-supplied desalination plant, ACS Sustain. Chem. Eng. 6 (2018) 14533–14541, https://doi.org/10.1021/acssuschemeng.8b03161.
[47] M. Herrero-Gonzalez, N. Admon, A. Dominguez-Ramos, R. Ibañez, A. Wolfson, A. Irabien, Environmental sustainability assessment of seawater reverse osmosis brine valorization by means of electrodialysis with bipolar membranes, Environ. Sci. Pollut. Res. 27 (2020) 1256–1266, https://doi.org/10.1007/s11356-019-04788-w.
[48] Siemens PSE, gPROMS Model Builder, Siemens PSE, 2023. https://www.psenterprise.com/ (accessed April 28, 2023).
[49] W. De Soto, S.A. Klein, W.A. Beckman, Improvement and validation of a model for photovoltaic array performance, Sol. Energy 80 (2006) 78–88, https://doi.org/10.1016/j.solener.2005.06.010.
[50] S. Petrana, E.A. Setiawan, A. Januardi, Solar panel performance analysis under Indonesian tropic climate using sandia PV array performance model and five parameter performance model, E3S Web Conf. 67 (2018) 1–11, https://doi.org/10.1051/e3sconf/20186702048.
[51] V. Lo Brano, G. Ciulla, An efficient analytical approach for obtaining a five parameters model of photovoltaic modules using only reference data, Appl. Energy 111 (2013) 894–903, https://doi.org/10.1016/j.apenergy.2013.06.046.
[52] V. Lo Brano, A. Orioli, G. Ciulla, A. Di Gangi, An improved five-parameter model for photovoltaic modules, Sol. Energy Mater. Sol. Cells 94 (2010) 1358–1370, https://doi.org/10.1016/j.solmat.2010.04.003.
[53] F. Rasool, M. Drieberg, N. Badruddin, B.S. Mahinder Singh, PV panel modeling with improved parameter extraction technique, Sol. Energy 153 (2017) 519–530, https://doi.org/10.1016/j.solener.2017.05.078.
[54] H. Ibrahim, N. Anani, Evaluation of analytical methods for parameter extraction of PV modules, Energy Procedia 134 (2017) 69–78, https://doi.org/10.1016/j.egypro.2017.09.601.
[55] D. Torres Lobera, S. Valkealahti, Dynamic thermal model of solar PV systems under varying climatic conditions, Sol. Energy 93 (2013) 183–194, https://doi.org/10.1016/j.solener.2013.03.028.
[56] S. Armstrong, W.G. Hurley, A thermal model for photovoltaic panels under varying atmospheric conditions, Appl. Therm. Eng. 30 (2010) 1488–1495, https://doi.org/10.1016/j.applthermaleng.2010.03.012.
[57] WATER-MINING, Water-Mining, EU, 2023. https://watermining.eu/. (Accessed 27 April 2023).
[58] Kyocera, KC200GT Photovoltaic Module Datasheet. http://www.kyocerasolar.com.au/, 2023.
[59] PVGIS, JRC's Directorate C: Energy, Transport and Climate – PVGIS, European Commission, 2023.
[60] C. Lei, Z. Li, Q. Gao, R. Fu, W. Wang, Q. Li, Z. Liu, Comparative study on the production of gluconic acid by electrodialysis and bipolar membrane electrodialysis: effects of cell configurations, J. Membr. Sci. 608 (2020) 118192, https://doi.org/10.1016/j.memsci.2020.118192.
[61] F. Giacalone, M. Papapetrou, G. Kosmadakis, A. Tamburini, G. Micale, A. Cipollina, Application of reverse electrodialysis to site-specific types of saline solutions: a techno-economic assessment, Energy 181 (2019) 532–547, https://doi.org/10.1016/j.energy.2019.05.161.
[62] Eurostat, Electricity Price Statistics, Eurostat, 2023. https://ec.europa.eu/eurostat/statistics-explained/index.php?title=Electricity_price_statistics#Electricity_prices_for_non-household_consumers. (Accessed 3 October 2023).
[63] H.S. Eggleston, L. Buendia, K. Miwa, T. Ngara, K. Tanabe, 2006 IPCC Guidelines for National Greenhouse Gas Inventories, Japan, 2006.
[64] Trading Economics, EU Carbon Permits, Trading Economics, 2023. https://tradingeconomics.com/commodity/carbon (accessed October 3, 2023).